

1 **A NON-UNIFORM CORROSION MODEL AND MESO-SCALE FRACTURE**
2 **MODELLING OF CONCRETE**

3
4 Xun Xi^{1,2}, Shangtong Yang^{2*} and Chun-Qing Li³

5 ¹ *School of Civil and Resource Engineering, University of Science and Technology Beijing, Beijing,*
6 *100083, China.*

7 ² *Department of Civil and Environmental Engineering, University of Strathclyde, Glasgow, G1 1XJ,*
8 *United Kingdom.*

9 ³ *School of Engineering, RMIT University, Melbourne, Vic 3001, Australia.*

10
11 **ABSTRACT**

12 Corrosion-induced concrete cracking is a significant durability problem for reinforced
13 concrete structures. Considerable research has been carried out in the last few decades to
14 understand and model the expansion mechanism of the corrosion products around the
15 reinforcing bar and simulate the cracking behaviour of the concrete cover. In this paper, a
16 new corrosion model based on non-uniform corrosion expansion is formulated and validated
17 against experimental data. A meso-scale fracture model, consisting of aggregates, cement
18 paste/mortar and ITZ, is established for the cases of both middle and side reinforcing bars.
19 Under the developed corrosion and concrete fracture model, the cracking phenomena of the
20 concrete cover are accurately simulated. It has been found that the non-uniform corrosion
21 model can be used to express the realistic corrosion rust progression around the reinforcing
22 bar, with the best accuracy. It has also been found that some microcracks occur before they
23 are connected to form the dominating discrete crack which usually appears on the concrete
24 surface. Moreover, the effects of the corrosion variables, as well as other key material and
25 geometric parameters, on surface cracking of concrete are investigated.

26 **Keywords:** non-uniform corrosion, cohesive crack model, meso-scale, reinforced concrete
27 structures, finite element method.

28 * Corresponding author. Tel: +44 141 548 3273. Email: shangtong.yang@strath.ac.uk.

29 1 INTRODUCTION

30 Reinforced concrete (RC) structures are widely used for civil structures and infrastructures,
31 e.g., buildings, bridges, retaining walls and tunnels. Concrete are normally considered a
32 durable material while corrosion of reinforcement has significant effects on the durability of
33 RC structures. Cracks induced by corrosion destroy the integrity of concrete cover, reduce the
34 reliability of concrete and lead to premature failure of RC structures and infrastructure.
35 Worldwide, the maintenance and repair costs for corrosion-affected concrete infrastructure
36 are estimated around \$100 billion per annum [1]. With regard to serviceability and timely
37 maintenance of the corrosion-affected RC structures and infrastructures, the engineers and/or
38 asset managers need better informed decisions.

39

40 Over the past two decades, considerable research has been carried out in understanding and
41 simulating the cracking mechanism of concrete cover induced by corrosion of reinforcement
42 [2-8]. Andrade et al. [2] indicated that a negligible loss (e.g., 20 μm) of the cross-section of
43 reinforcing bar could lead to a crack width of 0.05-0.1 mm, based on accelerated corrosion
44 tests. Liu and Weyers [3] modelled the surface cracking time of concrete cover due to
45 corrosion of reinforcement, taking the thickness of the “porous zone” around the
46 steel/concrete interface into account. Bhargava et al. [5, 6] proposed models for predicting the
47 time to cracking by considering the residual strength of cracked concrete and the stiffness
48 reduction. Li et al. [8] developed an analytical model to calculate the crack width of concrete
49 cover by assuming the cracks smeared in concrete and considering concrete as a quasi-brittle
50 material. Among these existing studies, most are focused on uniform or general corrosion of
51 the reinforcement.

52

53 Chlorides, as well as moisture and oxygen, diffuse into concrete and reach a threshold value
54 at the surface of steel bar, before the passive layer on steel surface is destroyed and corrosion
55 is initiated [9]. However, it is rare to have a uniform corrosion around the reinforcing bar, due
56 to different amount of chlorides, moisture and oxygen that are available on different sides of
57 the reinforcement; for example, the side of a reinforcing bar facing concrete cover should
58 have more sources to advance corrosion and hence more corrosion products accumulated on
59 this side. Recently, many researchers have started to model the cracking of concrete cover
60 induced by non-uniform corrosion of reinforcement. González et al. [10] perhaps first
61 compared the depth of pitting corrosion penetration on steel bar with the depth of general
62 corrosion and found that the maximum penetration of pitting corrosion on the steel bar is
63 equivalent to about three to sixteen times of the penetration of general corrosion. Jang and Oh
64 [11] extended the experimental results in [10] and designed a factor for the ratio of the
65 maximum thickness of non-uniform corrosion layer to the thickness of uniform corrosion
66 layer to express the non-uniform corrosion. Moreover, some researchers postulated corrosion
67 products followed a linear decrease distribution along the circle of steel bar [12, 13]. Pan and
68 Lu [14] proposed a non-linear corrosion model with a quadratic expansion function to model
69 the cracking of concrete induced by non-uniform corrosion. Further, Yuan and Ji [15]
70 conducted corrosion tests on RC samples by using artificial environmental chamber and
71 found the corrosion products distribution around the reinforcement is in a semi-elliptical
72 shape. Based on the semi-elliptical assumption, Yang et al. [16] proposed an analytical model
73 to calculate the time to cracking of concrete cover and Xi and Yang [17] developed a
74 numerical model to investigate cover cracking caused by corrosion of multiple reinforcing
75 bars. In addition, Zhao et al. [18-21] carried out corrosion tests on RC samples and proposed
76 a Gaussian non-uniform corrosion model to quantitatively define the corrosion products
77 distribution. Tran et al. [22] and Qiao et al. [23] proposed a non-uniform corrosion model by

78 considering uniform corrosion for part of rebar and no corrosion for the other part, according
79 to their results of experiments.

80

81 Once corrosion boundary model is established, the cracking of concrete caused by corrosion
82 of reinforcement can be simulated. Jang and Oh [11] simulated the stress to cracking of
83 concrete based on the linear decrease non-uniform corrosion model and Mohr-Coulomb
84 failure model. Zhao et al. [18] modelled the crack patterns of concrete based on Gaussian
85 non-uniform corrosion model and smeared crack model for concrete. Zhang et al. [24]
86 employed damage plasticity model to simulate the crack propagation of concrete based on
87 elliptical non-uniform corrosion model. However, most studies considered concrete as a
88 homogeneous material. The homogeneity assumption is only an approximation and, for more
89 accurate prediction, concrete should be treated as a three-phase heterogeneous material at the
90 mesoscale, consisting of cement paste/mortar, aggregate and interfacial transition zone (ITZ).
91 It has been found that the mechanical behaviour of the ITZ between aggregate and cement
92 paste has a significant effect on concrete strength and cracking prediction of concrete [25].
93 Du et al. [26] employed damage plasticity model to simulate the heterogeneous concrete
94 cracking patterns under elliptical non-uniform corrosion model [15]. Branko et al. [13] and
95 Chen et al. [12] built lattice models to simulate the time to cracking of heterogeneous
96 concrete cover based on the linear decrease corrosion model proposed by Jang and Oh [11].
97 However, amongst these limited literatures on modelling heterogeneous cracking of concrete
98 cover under non-uniform corrosion, almost none can predict discrete crack propagation and
99 micro-cracking prior to the formation of the dominating discrete crack.

100

101 This paper attempts to develop a new rational model for concrete cover cracking induced by
102 non-uniform corrosion of reinforcement. A novel non-uniform corrosion model is first

103 formulated based on von Mises distribution and validated against test data. The corrosion
104 model is then compared with existing non-uniform corrosion models in literatures, in terms of
105 accuracy of fitting experimental data, and the merit of the developed corrosion model is
106 discussed. Three parameters are modeled in the rust distribution function, i.e., the linear
107 relationship to corrosion degree λ , the non-uniform coefficient k and the location of the
108 maximum thickness of the corrosion rust layer μ . Under the expansion caused by corrosion of
109 reinforcement, two heterogeneous discrete crack models are built to simulate the concrete
110 cover cracking for the cases of middle rebar and corner rebar, respectively. The initial micro-
111 cracking and the subsequent dominating discrete crack propagation, and the surface crack
112 width development under various non-uniform corrosion coefficients are obtained. Moreover,
113 the effects of thickness of the “porous zone” on cracking patterns and surface crack width are
114 investigated.

115

116 **2 EXISTING NON-UNIFORM CORROSION MODELS**

117 In this section, all existing models on non-uniform corrosion rust distribution around the
118 reinforcing bar are briefly summarized. The thickness of corrosion rust layer $T_{cl}(\theta)$ consists
119 of two parts as shown in Figure 1(a), i.e., the corroded rebar with thickness $T_{co-st}(\theta)$ and the
120 expansion displacement beyond the original rebar with thickness $T_d(\theta)$. Thus, $T_{cl}(\theta)$ can be
121 expressed as follows:

$$122 \quad T_{cl}(\theta) = T_{co-st}(\theta) + T_d(\theta) \quad (1)$$

123

124 For clarification, it should be mentioned that some of the existing non-uniform corrosion
125 models are built based on the corrosion rust thickness distribution (i.e., $T_{cl}(\theta)$), e.g., [19, 22,

126 23], some based on the corroded steel bar (i.e., $T_{co-st}(\theta)$), e.g., [11, 15] and the others on the
 127 expansion displacement beyond the original bar (i.e., $T_d(\theta)$), e.g., [14].

128

129 According to the ratio α of rust expansion to corroded rebar, it can be approximately
 130 obtained as follows [27]:

$$131 \quad T_{cl}(\theta) = \alpha \times T_{co-st}(\theta) \quad (2)$$

132 By substituting Equation (2) into Equation (1), $T_d(\theta)$ can be derived as follows:

$$133 \quad T_d(\theta) = (\alpha - 1) \times T_{co-st}(\theta) \quad (3)$$

134 By substituting Equation (3) into Equation (2), $T_{cl}(\theta)$ can be obtained as follows:

$$135 \quad T_{cl}(\theta) = \frac{\alpha}{\alpha - 1} \times T_d(\theta) \quad (4)$$

136 By Equations (2-4), the non-uniform corrosion models can be linked up.

137

138 **2.1 Linear decrease corrosion model**

139 Jang and Oh [11] assumed that the maximum thickness of corrosion is at the location of rebar
 140 nearest the concrete surface (i.e., $\theta = \pi$) and the thickness of the corroded rebar $T_{co-st}(\theta)$ is
 141 linearly decreased from the outer region of the rebar. β is defined as the ratio of the maximum
 142 thickness of corroded rebar $T_{co-st,m}$ under non-uniform corrosion to the thickness of corroded
 143 rebar $T_{co-st,u}$ under uniform corrosion, given the same amount of corrosion products. As
 144 shown in Figure 1(b), the linear decrease corrosion model can be expressed as follows:

$$145 \quad T_{co-st}(\theta) = \begin{cases} \beta \times T_{co-st,u} \left(1 - \frac{\pi - \theta}{\pi - \theta_0}\right), & \theta_0 < \theta < \pi \\ \beta \times T_{co-st,u} \left(1 - \frac{\theta - \pi}{\pi - \theta_0}\right), & \pi \leq \theta < 2\pi - \theta_0 \\ 0, & 0 \leq \theta \leq \theta_0 \text{ \& } 2\pi - \theta_0 < \theta \leq 2\pi \end{cases} \quad (5)$$

146

147 Based on experimental results of González et al. [10] in which the value of β varies from

148 about 4 to 8 in natural condition, three special cases, i.e., $(\beta = 2, \theta_0 = 0)$, $(\beta = 4, \theta_0 = \frac{\pi}{2})$ and

149 $(\beta = 8, \theta_0 = \frac{3\pi}{4})$ were employed to simulate non-uniform corrosion [11-13].

150

151 2.2 Quadratic function corrosion model

152 Pan and Lu [14] proposed a nonlinear semicircle expansion displacement model with a

153 quadratic expansion function which can be expressed as follows:

$$154 \quad T_d(\theta) = 4 \times T_{d,m} \left[\frac{(\theta - \frac{\pi}{2})}{\pi} - \left(\frac{\theta - \frac{\pi}{2}}{\pi} \right)^2 \right], \quad \frac{\pi}{2} \leq \theta \leq \frac{3\pi}{2} \quad (6)$$

155 where $T_{d,m}$ is the maximum thickness of corrosion rust at $\theta = \pi$. The quadratic non-uniform

156 corrosion model is illustrated in Figure 1(c).

157

158 2.3 Partly uniform corrosion model

159 Qiao et al. [23] proposed a simple non-uniform corrosion model considering only part of the

160 rebar uniformly corroded, as shown in Figure 1(d). It can be expressed as follows:

$$161 \quad T_{cl}(\theta) = T_{cl}', \quad \theta_0 \leq \theta \leq 2\pi - \theta_0 \quad (7)$$

162 where T_{cl}' is the calculated thickness of corrosion layer to keep the amount of corrosion

163 products of the partly non-uniform corrosion the same as that of whole uniform corrosion. θ_0

164 is the un-corroded angle of steel bar.

165

166 2.4 Elliptical corrosion model

167 Yuan and Ji [15] found the corrosion products distribution around the reinforcement is in a
 168 semi-elliptical shape and proposed an elliptical corroded rebar model as shown in Figure 1(e).
 169 It could be expressed as follows:

$$170 \quad T_{co-st}(\theta) = R - \frac{R \cdot (R - T_{co-st,m})^2}{\sqrt{(R - T_{co-st,m})^2 \cdot \sin^2 \theta + (R)^2 \cdot \cos^2 \theta}}, \quad \frac{\pi}{2} \leq \theta \leq \frac{3\pi}{2} \quad (8)$$

171 where R is the radius of steel bar and $T_{co-st,m}$ is the maximum thickness of corroded steel bar.

172

173 **2.5 Gaussian corrosion model**

174 Zhao et al. [18-21] carried out accelerated corrosion tests on RC samples and proposed a
 175 Gaussian non-uniform corrosion model which can be expressed as follows:

$$176 \quad T_{cl}(\theta) = \frac{a_1}{a_2 \sqrt{2\pi}} e^{-\frac{(\theta-u)^2}{\sqrt{2}a_2}} + a_3 \quad (9)$$

177 where u is the location of the maximum thickness of corrosion layer which could be set as π
 178 [21]. a_1 is the non-uniform coefficient of the corrosion layer, a_2 is the spread coefficient of
 179 the corrosion layer and a_3 is the uniform coefficient of corrosion layer. As shown in Figure
 180 1(f), the function of corrosion products layer is displayed around the circumference of the
 181 original rebar in [18-21].

182

183 The existing five non-uniform corrosion models have been widely used to investigate the
 184 failure mechanism of RC structure covers under non-uniform corrosion assumption [10-16,
 185 18, 20-24, 26, 28, 29]. For linear decrease model [11], it may be difficult to build the
 186 relationship between the parameters β and θ under the same amount of corrosion products.

187 Therefore, existing studies only discussed three special cases for ($\beta = 2, \theta_0 = 0$),

188 ($\beta = 4, \theta_0 = \frac{\pi}{2}$) and ($\beta = 8, \theta_0 = \frac{3\pi}{4}$) [11-13]. For quadratic function model [14], the

189 function considers only half of steel bar corroded. The partly uniform corrosion model is
190 hypethetic and also the corrded angle is hard to determine. The elliptical corrosion model [15]
191 is obtained from slices of corroded RC samples, which showed only half of the steel bar was
192 corroded. However, the test results are limited and more data on a variety of corrosion
193 degrees should be conducted to justify the elliptical model. For the Gaussian model, the non-
194 uniform coefficient a_1 cannot accurately reflect the non-uniform level when the spread
195 coefficient a_2 is larger than 1.5 [21].

196

197 **3 A NEW CORROSION MODEL BASED ON VON MISES DISTRIBUTION**

198 Von Mises distribution is a continuous probability distribution on a circle, which is the
199 circular analogue of the normal distribution [30]. Von Mises distribution was first used to
200 study deviations of atomic weights from integer values and has become an important function
201 in the statistical theory [31].

202

203 By comparing all existing corrosion models, we have found the von Mises distribution could
204 be ideal to express the shape of corrosion progression. The corrosion rust layer thickness
205 $T_{cl}(\theta)$ can be formulated as follows:

$$206 \quad T_{cl}(\theta) = \lambda \frac{e^{k \cos(\theta - \mu)}}{2\pi I_0(k)} \quad (10)$$

207 where λ is a fitting parameter, μ is the location where the maximum thickness of corrosion
208 layer appears, $I_0(k)$ is the modified Bessel function of order 0 and k is the concentration
209 coefficient to define the level of non-uniform. The parameters will be discussed later in
210 details.

211

212 The total amount of corrosion products W can be expressed as follows:

213
$$W = W_m + W_s \quad (11)$$

214 where W_s is the amount of rust replacing the corroded steel with thickness $T_{co-st}(\theta)$ and W_m
 215 is the amount of rust expansion from the circumference of the origin rebar with thickness
 216 $T_d(\theta)$.

217

218 W_m can be obtained by an integration based on the radius of rebar:

219
$$W_m = \frac{1}{2} \int_0^{2\pi} (T_d(\theta) + R)^2 d\theta - \pi R^2 \quad (12)$$

220 Or,

221
$$W_m = \frac{1}{2} \int_0^{2\pi} (T_d(\theta)^2 + 2T_d R) d\theta \quad (13)$$

222 By neglecting the second order of small quantity, i.e., $T_d(\theta)^2$, W_m can be derived as follows:

223
$$W_m = \int_0^{2\pi} T_d(\theta) R d\theta \quad (14)$$

224 According to Equation (4), W_m can be rewritten as follows:

225
$$W_m = \int_0^{2\pi} \frac{\alpha - 1}{\alpha} T_{cl}(\theta) R d\theta \quad (15)$$

226 By substituting Equations (10) into Equation (15), it becomes:

227
$$W_m = \int_0^{2\pi} \frac{\alpha - 1}{\alpha} \lambda \frac{e^{k \cos(\theta - \mu)}}{2\pi I_0(k)} R d\theta \quad (16)$$

228 Further, it can be derived that:

229
$$W_m = \frac{\alpha - 1}{\alpha} R \lambda \int_0^{2\pi} \frac{e^{k \cos(\theta - \mu)}}{2\pi I_0(k)} d\theta \quad (17)$$

230 The integral part becomes the cumulative function of von Mises distribution in a whole circle
 231 and its value is 1. W_m can be expressed as follows:

232
$$W_m = \frac{\alpha - 1}{\alpha} R \lambda \quad (18)$$

233 The total amount of corrosion products W can be derived as follows:

$$234 \quad W = \alpha W_s \quad (19)$$

235 By substituting Equations (19) into Equation (11), W can also be expressed as follows:

$$236 \quad W = \frac{\alpha}{\alpha - 1} W_m \quad (20)$$

237 According to Equations (18) and (20), the total amount of corrosion products W can be
238 expressed as follows:

$$239 \quad W = R\lambda \quad (21)$$

240 It can be postulated that λ reflects directly the amount of corrosion products. It should be
241 noted that the formula is accurate when the radius loss of corroded rebar is relatively small
242 compared with the radius of origin rebar, which is the case in most engineering practice. It
243 has been reported a very small corrosion degree, i.e., 12 μm radius loss of rebar, can cause a
244 visible crack at surface of concrete cover [32]. Therefore, such a hypothesis of the von Mises
245 model is well justified.

246

247 According to Equations (10) and (21), the corrosion layer thickness $T_{cl}(\theta)$ can be derived as
248 follows:

$$249 \quad T_{cl}(\theta) = \frac{W}{R} \times \frac{e^{k \cos(\theta - \mu)}}{2\pi I_0(k)} \quad (22)$$

250 The corrosion degree of reinforcement η can be expressed as follows:

$$251 \quad \eta = \frac{W_s}{W_0} \times 100\% \quad (23)$$

252 where the W_0 is the original amount of the reinforcing steel.

253

254 According to Equations (19) and (22-23), the corrosion layer thickness $T_{cl}(\theta)$ can be written
255 as a function of corrosion degree:

$$256 \quad T_{cl}(\theta) = \alpha\pi R\eta \times \frac{e^{k\cos(\theta-\mu)}}{2\pi I_0(k)} \quad (24)$$

257 Therefore, the parameter λ has a linear relationship with corrosion degree η , and λ can be
258 defined as the corrosion degree indicator.

259

260 **4 VALIDATION, COMPARISONS AND PARAMETERS**

261 To verify the proposed von Mises corrosion distribution model, test data on non-uniform
262 corrosion development are searched and collected in a comprehensive manner. Figure 2
263 shows the regression analysis of the proposed von Mises model with the test data [15, 19, 23].
264 It should be mentioned that, the results from Qiao et al. [23] used corroded rebar thickness
265 $T_{co-st}(\theta)$, while the data in other literature studies were based on the thickness of corrosion
266 products layer $T_{cl}(\theta)$. The fitting parameters and R^2 (coefficient of determination) values for
267 the test data are shown in Table1. It can be found that most values of R^2 are larger than 0.9.
268 The R^2 of data 8 is 0.768, which is caused by significant crack width (i.e., 0.4 mm). It can be
269 proved that, prior to occurrence of any significant crack, the von Mises model can predict the
270 non-uniform corrosion progression very well.

271

272 The regression analysis of elliptical model [15], linear decrease model [11, 12], quadratic
273 expansion model [14], Gaussian model [19] and the developed von Mises model with the test
274 data in terms of $T_{cl}(\theta)$ are illustrated in Figure 3. It can be found the curves predicted by the
275 developed von Mises model are closest to the experimental data. The average R^2 against the
276 six groups of test data for the existing non-uniform models and the von Mises model are

277 compared and shown in Figure 4. It can be seen that the von Mises model has the best
278 accuracy in fitting with the experimental data. Meanwhile, the von Mises model can be
279 regarded as a circular analogue of Gaussian model but leads to better prediction of corrosion
280 rust distribution around the reinforcing bar. In addition, the von Mises model has less number
281 of parameters in formulating the non-uniform corrosion rust progression and these parameters
282 also have direct physical meanings.

283

284 As introduced in the experiments [15, 19, 23], the test data 4 and 6 were obtained from
285 corrosion of corner rebar while the others were from corrosion of middle rebar. The polar
286 coordinate system and the location of maximum thickness of corrosion layer in the
287 experiments [15, 19, 23] are shown in Figure 5. From fitting results by von Mises model, the
288 value of μ is near π , which means the von Mises model can describe the location of maximum
289 thickness of corrosion layer well. As a corrosion model used to analyse cracking of concrete
290 cover induced by non-uniform corrosion of reinforcement, the parameter μ can be set as π in
291 the polar coordinate system.

292

293 In the von Mises distribution k is the concentration coefficient and the smaller the k is, the
294 distribution will be more close to uniform. From the fitting results with the test data, the value
295 of k varies from 0.555 to 3.362. To investigate the effect of k on corrosion layer distribution
296 in the von Mises corrosion model, the corrosion layer distribution under four values of k are
297 produced and plotted in Figure 6. It should be noted that the right figures in Figure 6 show
298 the front of the corrosion layer based on a circle representing the original rebar, not the
299 expansion displacements of corrosion products. When k is zero, the corrosion layer thickness
300 $T_{cl}(\theta)$ becomes a constant value and the von Mises corrosion model describes uniform

301 corrosion. Therefore, $k=0$ is a special case which represents uniform corrosion while all other
302 values of k (must be positive) define non-uniform corrosion.

303

304 In real corrosion propagation process, the non-uniform coefficient k may not be a constant
305 but varying along time. There is very limited experimental and observational data available
306 which cannot warrant a thorough understanding and elaboration about k . However, in this
307 study, it has been found that for most existing data larger value of λ leads to smaller k .
308 Moreover, it is considered that when corrosion progresses, the non-uniform coefficient will
309 be smaller and smaller, i.e. the corrosion will become more close to uniform. Nonetheless, it
310 has not been proved yet and hard to predict the varying value of k under different corrosion
311 degrees. The value of k may be related to chloride content, geometry of RC structures,
312 corrosion degree and surface crack of concrete. As chlorides, moisture and oxygen diffuse
313 into concrete, a small part of rebar near concrete cover first corrodes. The rusts gradually
314 form which fill in the voids around steel/concrete interface and expand outwards. At this
315 moment, the non-uniform coefficient k can be large. With the corrosion propagation, more
316 regions of rebar start to corrode and more microcell corrosion forms. The non-uniform
317 coefficient k will then decrease. In particular, after crack penetrates the concrete cover and
318 the chloride and oxygen can subsequently reach the rebar directly, the rebar perhaps corrode
319 almost homogeneously around its whole circumference. Having said this, it is possible that,
320 before a significant crack forms, the non-uniform coefficient is in a range which means the
321 cracking of concrete is always induced by a typical non-uniform corrosion. More researches
322 are necessary, especially experimental results, to clarify the effects of different underlying
323 parameters on k and then formulate an analytical function for k . Figure 7 shows the corrosion
324 rust distribution under the varying k and corrosion degrees. It can be seen that, as corrosion
325 progresses, the distribution of corrosion rust approaches uniform when k decreases.

326

327 $T_d(\theta)$ is used as the displacement boundary condition in modelling the cracking of concrete
328 cover. According to Equations (4) and (24), $T_d(\theta)$ can be expressed as follows:

329
$$T_d(\theta) = (\alpha - 1)\pi R \eta \times \frac{e^{k \cos(\theta - \mu)}}{2\pi d_0(k)} \quad (25)$$

330 When the corrosion process starts, corrosion rusts first fill in the annular porous layer in
331 concrete around the reinforcing bar, often referred to as “porous zone”. This initial stage
332 normally does not produce stresses in concrete. Taking into account the “porous zone” with
333 thickness T_0 , the displacement boundary condition $T_d(\theta)$ can be modified as follows:

334
$$T_d(\theta) = \left\langle (\alpha - 1)\pi R \eta \times \frac{e^{k \cos(\theta - \mu)}}{2\pi d_0(k)} - T_0 \right\rangle \quad (26)$$

335 where $\langle \rangle$ is the Macaulay bracket which means the displacement expansion boundary $T_d(\theta)$
336 will be regarded as zero if the value is less than zero. Figure 8 shows the expansion
337 displacement $T_d(\theta)$ as a function of θ under different values of non-uniform coefficient k .
338 The input parameters are listed in Table 2. The corrosion products accumulate from 150° to
339 210° for $k=25$, 120° to 240° for $k=5$, 90° to 270° for $k=2$, 60° to 300° for $k=1.1$ and uniform
340 corrosion for $k=0$, respectively. Although the total amount of corrosion products for each of
341 the above-mentioned cases is the same, the expansion amount of corrosion products W_m is
342 different because of different amount of corrosion products filling in the “porous zone”.

343

344 Some researchers have tried to describe the localised or pitting corrosion by a factor of the
345 maximum pitting penetration over the corrosion thickness of general corrosion [10-13]. It has
346 been found that this factor ranges from about 4 to 8 in natural conditions and 5 to 13 in
347 accelerated testing of reinforced concrete. In this model, a factor β is expressed as follows:

348
$$\beta = \frac{T_{co-st,k}(\pi)}{T_{co-st,k=0}(\pi)} \quad (27)$$

349 Where $T_{co-st,k}(\pi)$ is the maximum corroded rebar thickness of non-uniform corrosion and
 350 $T_{co-st,k=0}(\pi)$ is the corroded rebar thickness of uniform corrosion. According to Equations (2)
 351 and (24), $T_{co-st,k}(\pi)$ and $T_{co-st,k=0}(\pi)$ can be derived respectively as follows:

352
$$T_{co-st,k}(\pi) = \pi R \eta \times \frac{e^k}{2\pi I_0(k)} \quad (28)$$

353
$$T_{co-st,k=0}(\pi) = \pi R \eta \times \frac{1}{2\pi I_0(0)} \quad (29)$$

354 By substituting Equations (28) and (29) into Equation (27), β can be expressed as follows:

355
$$\beta = \frac{e^k}{2\pi I_0(k)} \times 2\pi I_0(0) \quad (30)$$

356 β can be calculated via Equation (30) and compared with k originally proposed in this study,
 357 as shown in Figure 8(a).

358

359 **5 MESO-SCALE DISCRETE CRACK MODEL FOR FRACTURE OF CONCRETE**

360 In this paper, concrete is modelled as a three-phase (i.e., consisting of mortar, aggregates and
 361 ITZ) material. The shape of aggregate is simplified to a random polygon with 3-7 sides. The
 362 aggregate size distribution can be represented by a grading curve, which is usually expressed
 363 in terms of cumulative percentage passing through a series of sieves with different opening
 364 sizes. A typical gradation of aggregate size distribution is listed in Table 3 [33]. For
 365 simplicity, only coarse aggregates larger than 2.4 mm are modelled in this study, while fine
 366 aggregates and cement are treated as mortar phase. Coarse aggregates generally occupy 40%
 367 of the whole volume of concrete. A similar algorithm for generating polygonal aggregate

368 proposed by Pan et al. [34] is devised in this study. There is no overlapping of aggregates in
369 the generation process. The script for producing the 3-phase structure is written in Python
370 which controls the drawings in AutoCAD; the structure is then imported into FE software
371 (i.e., ABAQUS) for analysis.

372

373 Figure 9 shows the mesh of the meso-scale RC cover structure with middle and corner rebars.
374 The size of the RC structure is set 150×150 mm and the thickness of concrete cover is 40 mm.
375 Two types of elements are employed in this study, i.e., a 4-node cohesive element for
376 interfaces between the triangle elements and a 3-node plane strain element for the bulk mortar
377 and aggregates. To model arbitrary cracking in concrete, the cohesive elements are embedded
378 at the interfaces throughout the mesh; very fine mesh is produced to ensure random crack
379 paths. The insertion process of cohesive elements is accomplished by an in-house script
380 written in Python. First, all individual nodes are replaced by certain number of new nodes at
381 the same location. The number of newly created nodes depends on the number of the
382 elements connecting to the original node. Second, the newly created nodes at the interface
383 between two triangle elements are identified and linked to form a cohesive element. Figure
384 10 shows the inserted cohesive elements at the interface of aggregate and mortar, as well as
385 in the aggregates and the mortar. Therefore, the developed model is capable of simulating
386 crack propagation both at the interface and in the bulk mortar and aggregates, depending on
387 their material properties. However, the mechanical properties of aggregates are normally
388 considerably stronger than mortar and the ITZ; thus it is in general very rare to have a crack
389 breaking through an aggregate. In this paper, fracture properties are only assigned in the ITZ
390 and mortar to simulate cracking, in light of reducing computational cost. The numbers of
391 elements for the two models, i.e., cases for corner and middle rebars respectively, are shown
392 in Table 4.

393

394 Under the expansive force induced by the accumulation of corrosion products, the concrete
395 cover is predominantly controlled by tension failure and shear failure in case of non-uniform
396 expansion. Therefore, the compressive property of concrete can be assumed elastic without
397 defining the compression failure. Different from some special cases where shearing is not an
398 issue (e.g., [35]), the shearing properties of the material phases affect the cracking paths and
399 structural failure under heterogeneous assumption [36]. Due to the lack of experimental data,
400 the shear strength and Mode-II fracture energy were assumed to be the same as these of
401 Mode-I [25, 37, 38]. The constitutive stress-displacement relation ($\sigma - \delta$) under tension, can
402 be shown in Figure 11. The tensile stress linearly increases until its maximum value, i.e.,
403 tensile strength f_t' ; such a linearity is determined by a penalty stiffness K_p . After reaching the
404 peak value, the tensile stress decreases, following certain strain softening rules, e.g., linear,
405 bi-linear, exponential, etc. The area underneath the curve in Figure 12 is known as the
406 fracture energy G_f . As discussed, aggregate is assumed elastic without defining its damage
407 properties.

408

409 The fracture properties of ITZ play an important role in meso scale fracture modelling of
410 concrete [25, 39]. However, it is very hard to obtain the tensile strength and fracture energy
411 of ITZ by experimental tests. Very limited experimental results indicated that the tensile
412 strength of ITZ is about 1/16 to 3/4 of the strength of mortar [39, 40]. Rao and Prasad found
413 the fracture toughness of ITZ varies from 4% to 34% of mortar which is affected by the
414 roughness of aggregates [40]. Tregger et al. found the fracture energy of ITZ is about 0.5
415 time of that of mortar by experiments [41]. Some researchers simulated the meso scale
416 fracture of concrete under direct tension load and assumed the tensile strength and fracture
417 energy of ITZ both are 0.5 time of those of mortar [25, 37]. Therefore, the tensile strength of

418 ITZ is regarded as 0.5 time of that of mortar in this paper. Due to the failure of ITZ is more
419 brittle than mortar [42], the fracture energy of ITZ is assumed as 0.25 time of that of mortar.
420 The values for all the basic parameters are shown in Table 5. It should be mentioned the
421 effect of aggregate size and roughness on properties of ITZ is not considered in this paper.

422

423 **6 SIMULATION RESULTS AND DISCUSSION**

424 Figure 12 shows the crack propagation process induced by corrosion of the middle rebar for
425 non-uniform coefficient $k=2$. Cohesive elements with damage variable D equal to 1 (i.e.
426 complete failure) are plotted in red. It can be found that a few micro cracks are first initiated
427 at the aggregate-mortar interfaces near the top surface of the concrete cover. As corrosion
428 continues, the micro cracks are then connected to form a dominant crack propagating from
429 the concrete surface to the rebar. The phenomenon that a crack propagates from concrete
430 surface towards the reinforcement has a good agreement with the experiments [43]. When the
431 corrosion degree increases to 0.15%, new micro cracks are generated at the aggregate-mortar
432 interfaces at the right of the rebar. Finally, three macro cracks are formed, as shown in Figure
433 12(d). Amongst these three discrete cracks, the top one has the largest opening. Unlike
434 macroscale fracture modelling which considers concrete as a homogeneous material [17],
435 micro cracks always start first at the ITZ before they are connected and form a macro discrete
436 crack. This is because the strength and fracture energy of ITZ cohesive elements are
437 significantly lower than those of mortar. As such, the developed meso-scale fracture model is
438 advantageous compared with most existing concrete fracture models [27, 36] in terms of
439 capturing microcracks in different material phases prior to the occurrence of any dominating
440 visible cracks. It has been found that the effect of aggregate randomness on concrete tensile
441 strength and softening is limited [37, 38]. As the corrosion develops to the stage where the
442 tensile stress reaches the tensile strength, concrete is cracked. The aggregate randomness

443 almost has no effect on the initial cracking. Further, crack deflection will occur when the
444 crack path is around an aggregate or a weaker ITZ. However, the general crack pattern and
445 crack width is quite close to each other under the same aggregate fraction, grading curve and
446 non-uniform corrosion coefficient.

447

448 The cracking patterns under different corrosion non-uniform coefficient k are plotted in
449 Figure 13. It should be mentioned that the computational simulations do not converge for
450 $k=25$ beyond corrosion degree 0.08% and $k=5$ beyond corrosion degree 0.23%, respectively,
451 due to severe local damage. It can be found that the non-uniform coefficient of corrosion has
452 a significant effect on the cracking patterns of the concrete cover. For $k=0$, i.e., uniform
453 corrosion, two cracks appear, as shown in Figure 13(a). The top crack is the dominant crack
454 while the other one develops after the top crack. For uniform corrosion, the location of the
455 surface crack may be related to the shape and size of aggregates, cover thickness and
456 diameter of rebar. For non-uniform corrosion of middle rebar, there are three cracks, namely,
457 top crack, left crack and right crack. It has been found that the larger the non-uniform
458 coefficient is, the left and right cracks are closer to the top surface of concrete cover. When
459 the non-uniform coefficients are 5 and 25, the left and right cracks are located near the
460 horizontal line which causes delamination failure of the cover. This phenomenon has a good
461 agreement with the crack patterns found in Malumbela's experiments [44].

462

463 Crack width is an important parameter with regards to the durability of concrete structures.
464 Upon measuring the distances between the nodes of specific cohesive elements of the surface
465 cracks, the crack width evolution of the surface cracks as a function of corrosion degree for
466 different non-uniform coefficients are shown in Figure 14. It can be seen that the surface
467 crack suddenly increases to about 0.03 mm; after that, the surface crack width grows up

468 almost linearly. A very small corrosion degree (less than 0.25%) can cause concrete cover
469 cracking. Moreover, it has been found that the larger the non-uniform coefficient is, the
470 smaller the corrosion degree at surface cracking is. Although the final crack width for $k=25$
471 and $k=0$ is small, it can be predicted that more uniform corrosion can lead to smaller crack
472 width under given corrosion degree. Most previous studies [1, 3, 6, 7, 45] assumed uniform
473 corrosion which overestimated the volume that is occupied by corrosion products and
474 therefore underestimated the time to surface cracking and crack width development.

475

476 Figure 15 illustrates the crack propagation process induced by corrosion of the corner rebar
477 for non-uniform coefficient $k=2$. As discussed, micro cracks are first initiated at the
478 aggregate-mortar interfaces at the right of the rebar before a dominant crack forms. The other
479 crack appears at the upper left corner of rebar and continues to propagate to the surface of
480 concrete.

481

482 The cracking patterns induced by corrosion of corner rebar under different corrosion non-
483 uniform coefficient k are plotted in Figure 16. The computation did not converge for $k=25$
484 beyond the corrosion degree 0.10%. For uniform corrosion, there are two macro cracks at
485 right side of the rebar and one macro crack at top of the rebar. The cracking pattern for
486 uniform corrosion is related to the size and shape of aggregates and the cracks will cause a
487 spalling failure of the concrete cover. For non-uniform corrosion, larger non-uniform
488 coefficient can cause the incline of the macro cracks towards the maximum thickness of the
489 corrosion layer (i.e., $\theta=\pi$) and the angle of the spalling failure becomes smaller. Further, for a
490 relatively large non-uniform coefficient, some micro cracks appear around the maximum
491 thickness of corrosion layer, which conforms to the experimental results in Zhao et al. [20].

492

493 Figure 17 shows the surface crack width as a function of corrosion degree under different
494 non-uniform coefficients for the corner rebar case. When the non-uniform coefficient
495 increases from 0 to 25, the corrosion degree to cause surface cracking is decreased from
496 about 0.21% to 0.05%. It has been found that larger non-uniform coefficient can lead to
497 greater slope of curve of surface crack width as a function of corrosion degree. This means
498 that, given the same corrosion degree, the crack width for more localised corrosion is larger
499 than that for uniform corrosion.

500

501 It has been reported that the thickness of the “porous zone” between reinforcement and
502 concrete considerably affect the cracking of concrete cover [16]. Figure 18 illustrates the
503 effect of thickness of the “porous zone” on the cracking pattern. It can be seen that as the
504 thickness of the “porous zone” (T_0) increases, the crack widths for all three discrete cracks
505 reduce. Moreover, the two side cracks tend to incline towards the top surface, when T_0
506 increases. Figure 19 shows the effect of T_0 on surface crack width for corrosion non-uniform
507 coefficient $k=0$ and 2. It can be seen that, for a large thickness of “porous zone”, more
508 corrosion products are required to fracture the concrete cover. When T_0 increases by 12.5 μm ,
509 the corrosion degree to surface cracking increases by about 0.05% for $k=2$ and 0.10% for
510 $k=0$. Therefore, the effect of thickness of the “porous zone” on surface crack width varies
511 from corrosion non-uniform coefficient. The smaller the corrosion non-uniform coefficient is,
512 the thickness of the “porous zone” affects the corrosion degree to surface cracking more
513 significantly. It should be mentioned that, the value of T_0 is a virtual concept for calculating
514 the corrosion-accommodating region, which is related to water/cement ratio and corrosion
515 rate [46]. For non-uniform corrosion with different non-uniform coefficients, the corrosion
516 products required for filling in the “porous zone” are different.

517

518 7 CONCLUSIONS

519 In this paper, a von Mises corrosion model was derived to formulate the corrosion expansion
520 around the reinforcing bar. The model was simply composed of three parameters including
521 the corrosion degree indicator λ , the non-uniform coefficient k and the location of the
522 maximum thickness of the corrosion layer μ . The results predicted by the developed model
523 have been compared with experimental results and a good agreement has been achieved.
524 Compared with the existing models, the von Mises model has the best accuracy in fitting with
525 the experimental data and fewer parameters with direct physical meanings. Moreover, the
526 thickness of the “porous zone” between reinforcement and concrete has also been taken into
527 account. Two meso-scale models consisting of aggregates, mortar and ITZ were built for the
528 cases of the middle and corner rebars, respectively. The concrete cover cracking induced by
529 corrosion of the middle and corner bars with five different non-uniform coefficients were
530 simulated. Moreover, the crack width developments as a function of corrosion degree were
531 obtained. It has been found that the larger the non-uniform coefficient is, the smaller the
532 corrosion degree at surface cracking is. It has also been found that the thickness of the
533 “porous zone” can dramatically change the amount of rust that is required to fracture the
534 concrete cover; meanwhile, the smaller the non-uniform coefficient is, the more the thickness
535 of the “porous zone” affects the corrosion degree to the surface cracking.

536

537 ACKNOWLEDGEMENTS

538 Financial support from European Commission via the Marie Skłodowska-Curie H2020 RISE
539 scheme under 645696 and National Key R&D Plan of China (Grant No: 2016YFC0600803)
540 is gratefully acknowledged. The first author would also like to thank China Scholarship
541 Council for supporting his PhD research at the University of Strathclyde, UK.

543 REFERENCES

- 544 [1] C.Q. Li, S.T. Yang, Prediction of concrete crack width under combined reinforcement
545 corrosion and applied load, *Journal of Engineering Mechanics-ASCE*, 137 (2011) 722-731.
- 546 [2] C. Andrade, F.J. Molina, C. Alonso, Cover cracking as a function of rebar corrosion: Part
547 1-experiment test, *Materials and Structures*, 26 (1993) 453-454.
- 548 [3] Y. Liu, R.E. Weyers, Modelling the time-to-corrosion cracking in chloride contaminated
549 reinforced concrete structures, *ACI Materials Journal*, 95 (1998) 675-681.
- 550 [4] S.J. Pantazopoulou, K.D. Papoulia, Modeling cover cracking due to reinforcement
551 corrosion in RC structures, *Journal of Engineering Mechanics-ASCE*, 127 (2001) 342-351.
- 552 [5] K. Bhargava, A.K. Ghosh, Y. Mori, S. Ramanujam, Model for cover cracking due to rebar
553 corrosion in RC structures, *Engineering Structures*, 28 (2006) 1093-1109.
- 554 [6] K. Bhargava, A.K. Ghosh, Y. Mori, S. Ramanujam, Modeling of time to corrosion-
555 induced cover cracking in reinforced concrete structures, *Cement and Concrete Research*, 35
556 (2005) 2203-2218.
- 557 [7] C. Lu, W. Jin, R. Liu, Reinforcement corrosion-induced cover cracking and its time
558 prediction for reinforced concrete structures, *Corrosion Science*, 53 (2011) 1337-1347.
- 559 [8] C.Q. Li, R.E. Melchers, J.J. Zheng, Analytical model for corrosion-induced crack width in
560 reinforced concrete structures, *ACI Structural Journal*, 103 (2006) 479-487.
- 561 [9] C. Cao, M.M.S. Cheung, B.Y.B. Chan, Modelling of interaction between corrosion-
562 induced concrete cover crack and steel corrosion rate, *Corrosion Science*, 69 (2013) 97-109.
- 563 [10] J.A. González, C. Andrade, C. Alonso, S. Feliu, Comparison of rates of general
564 corrosion and maximum pitting penetration on concrete embedded steel reinforcement,
565 *Cement and Concrete Research*, 25 (1995) 257-264.
- 566 [11] B.S. Jang, B.H. Oh, Effects of non-uniform corrosion on the cracking and service life of
567 reinforced concrete structures, *Cement and Concrete Research*, 40 (2010) 1441-1450.
- 568 [12] A. Chen, Z. Pan, R. Ma, Mesoscopic simulation of steel rebar corrosion process in
569 concrete and its damage to concrete cover, *Structure and Infrastructure Engineering*, 13
570 (2016) 478-493.
- 571 [13] B. Šavija, M. Luković, J. Pacheco, E. Schlangen, Cracking of the concrete cover due to
572 reinforcement corrosion: A two-dimensional lattice model study, *Construction and Building
573 Materials*, 44 (2013) 626-638.
- 574 [14] T. Pan, Y. Lu, Stochastic Modeling of Reinforced Concrete Cracking due to Nonuniform
575 Corrosion: FEM-Based Cross-Scale Analysis, *Journal of Materials in Civil Engineering*, 24
576 (2012) 698-706.
- 577 [15] Y. Yuan, Y. Ji, Modeling corroded section configuration of steel bar in concrete
578 structure, *Construction and Building Materials*, 23 (2009) 2461-2466.
- 579 [16] S.T. Yang, K.F. Li, C.Q. Li, Analytical model for non-uniform corrosion-induced
580 concrete cracking, *Magazine of Concrete Research*, 90 (2018) 1-10.
- 581 [17] X. Xi, S. Yang, Time to surface cracking and crack width of reinforced concrete
582 structures under corrosion of multiple rebars *Construction and Building Materials*, 155 (2017)
583 114-125.
- 584 [18] Y. Zhao, A.R. Karimi, H.S. Wong, B. Hu, N.R. Buenfeld, W. Jin, Comparison of
585 uniform and non-uniform corrosion induced damage in reinforced concrete based on a
586 Gaussian description of the corrosion layer, *Corrosion Science*, 53 (2011) 2803-2814.

587 [19] Y. Zhao, B. Hu, J. Yu, W. Jin, Non-uniform distribution of rust layer around steel bar in
588 concrete, *Corrosion Science*, 53 (2011) 4300-4308.

589 [20] Y. Zhao, J. Yu, B. Hu, W. Jin, Crack shape and rust distribution in corrosion-induced
590 cracking concrete, *Corrosion Science*, 55 (2012) 385-393.

591 [21] Y. Zhao, X. Zhang, H. Ding, W. Jin, Non-uniform distribution of a corrosion layer at a
592 steel/concrete interface described by a Gaussian model, *Corrosion Science*, 112 (2016) 1-12.

593 [22] K.K. Tran, H. Nakamura, K. Kawamura, M. Kunieda, Analysis of crack propagation due
594 to rebar corrosion using RBSM, *Cement and Concrete Composites*, 33 (2011) 906-917.

595 [23] D. Qiao, H. Nakamura, Y. Yamamoto, T. Miura, Crack patterns of concrete with a single
596 rebar subjected to non-uniform and localized corrosion, *Construction and Building Materials*,
597 116 (2016) 366-377.

598 [24] J. Zhang, X. Ling, Z. Guan, Finite element modeling of concrete cover crack
599 propagation due to non-uniform corrosion of reinforcement, *Construction and Building*
600 *Materials*, 132 (2017) 487-499.

601 [25] W. Ren, Z. Yang, R. Sharma, C. Zhang, P.J. Withers, Two-dimensional X-ray CT image
602 based meso-scale fracture modelling of concrete, *Engineering Fracture Mechanics*, 133
603 (2015) 24-39.

604 [26] X. Du, L. Jin, R. Zhang, Modeling the cracking of cover concrete due to non-uniform
605 corrosion of reinforcement, *Corrosion Science*, 89 (2014) 189-202.

606 [27] E. Chen, C.K.Y. Leung, Finite element modeling of concrete cover cracking due to non-
607 uniform steel corrosion, *Engineering Fracture Mechanics*, 134 (2015) 61-78.

608 [28] L. Jin, R. Zhang, X. Du, Y. Li, Investigation on the cracking behavior of concrete cover
609 induced by corner located rebar corrosion, *Engineering Failure Analysis*, 52 (2015) 129-143.

610 [29] X. Ning, R. Qingwen, P. Joe, Y.L. Robert, P. Anil, Nonuniform Corrosion-Induced
611 Stresses in Steel-Reinforced Concrete, *Journal of Engineering Mechanics*, ASCE, 138 (2012)
612 338-346.

613 [30] C. Forbes, M. Evans, N. Hastings, B. Peacock, *Statistical Distributions*, Fourth ed., John
614 Wiley & Sons, Inc.2010.

615 [31] D.J. Best, N.I. Fisher, Efficient Simulation of the von Mises Distribution, *Journal of the*
616 *Royal Statistical Society. Series C (Applied Statistics)*, 28 (1979) 152-157.

617 [32] C. E, Computational modeling of concrete cracking due to non-uniform steel corrosion
618 in reinforced concrete structures, The Hong Kong University of Science and Technology,
619 2015.

620 [33] A.M. Neville, *Properties of concrete*, Fourth ed., Pearson Education Limited, London,
621 2006.

622 [34] Z. Pan, X. Ruan, A. Chen, A 2-D numerical research on spatial variability of concrete
623 carbonation depth at meso-scale, *Computers and Concrete*, 15 (2015) 231-257.

624 [35] J.C. Gálvez, D.A. Cendón, J. Planas, Influence of shear parameters on mixed-mode
625 fracture of concrete, *International Journal of Fracture*, 118 (2002) 163-189.

626 [36] Z. Yang, X. Frank Xu, A heterogeneous cohesive model for quasi-brittle materials
627 considering spatially varying random fracture properties, *Computer Methods in Applied*
628 *Mechanics and Engineering*, 197 (2008) 4027-4039.

629 [37] Z.J. Yang, X.T. Su, J.F. Chen, G.H. Liu, Monte Carlo simulation of complex cohesive
630 fracture in random heterogeneous quasi-brittle materials, *International Journal of Solids and*
631 *Structures*, 46 (2009) 3222-3234.

632 [38] X.F. Wang, Z.J. Yang, J.R. Yates, A.P. Jivkov, C. Zhang, Monte Carlo simulations of
633 mesoscale fracture modelling of concrete with random aggregates and pores, *Construction*
634 *and Building Materials*, 75 (2015) 35-45.

- 635 [39] J. Xiao, W. Li, D.J. Corr, S.P. Shah, Effects of interfacial transition zones on the stress–
636 strain behavior of modeled recycled aggregate concrete, *Cement and Concrete Research*, 52
637 (2013) 82-99.
- 638 [40] G.A. Rao, B.K. Raghuprasad, Influence of type of aggregate and surface roughness on
639 the interface fracture properties, *Materials and Structures*, 37 (2004) 328-334.
- 640 [41] N. Tregger, D. Corr, L. Graham-Brady, S. Shah, Modeling the effect of mesoscale
641 randomness on concrete fracture, *Probabilistic Engineering Mechanics*, 21 (2006) 217-225.
- 642 [42] D. Corr, M. Accardi, L. Graham-Brady, S. Shah, Digital image correlation analysis of
643 interfacial debonding properties and fracture behavior in concrete, *Engineering Fracture*
644 *Mechanics*, 74 (2007) 109-121.
- 645 [43] S. Caré, Q.T. Nguyen, K. Beddiar, Y. Berthaud, Times to cracking in reinforced mortar
646 beams subjected to accelerated corrosion tests, *Materials and Structures*, 43 (2009) 107-124.
- 647 [44] G. Malumbela, P. Moyo, M. Alexander, Influence of corrosion crack patterns on the rate
648 of crack widening of RC beams, *Construction and Building Materials*, 25 (2011) 2540-2553.
- 649 [45] C.Q. Li, Time Dependent Reliability Analysis of the Serviceability of Corrosion
650 Affected Concrete Structures, *International Journal of Materials and Structural Reliability*, 3
651 (2005) 105-116.
- 652 [46] A. Jamali, U. Angst, B. Adey, B. Elsener, Modeling of corrosion-induced concrete cover
653 cracking: A critical analysis, *Construction and Building Materials*, 42 (2013) 225-237.
- 654

655 **LIST OF TABLES**

656 1. Values of basic parameters formulated in the developed von Mises corrosion model

657 2. Values of basic variables used in the example

658 3. Three-segment gradation of aggregate size distribution [33]

659 4. Number of elements in the computational models

660 5. Values for geometric and mechanical parameters for different phases

661

662 Table 1 Values of basic parameters formulated in the developed von Mises corrosion model

Test data	λ	k	μ	R^2	Test data	λ	k	μ	R^2
1	0.321	3.122	3.181	0.991	5	0.613	3.362	3.348	0.817
2	0.941	0.555	3.188	0.934	6	0.353	3.232	3.182	0.906
3	0.198	1.832	3.325	0.931	7	0.799	0.923	2.963	0.953
4	0.349	3.285	3.173	0.901	8	1.550	0.689	3.540	0.768

663

664

665

666

Table 2 Values of basic variables in the example

Symbol	Values	Sources
R	8 mm	Zhao [19]
T_0	12.5 μm	Liu and Weyers [3]
α	3.83	Liu and Weyers [3, 4]
η	0.26%	Zhao [19]

667

668

669

Table 3 Three-segment gradation of aggregate size distribution [33]

Aggregate size (mm)	Fraction (%)
2.40-4.76	20.2 %
4.76-9.52	39.9%
9.52-19.05	39.9%

670

671

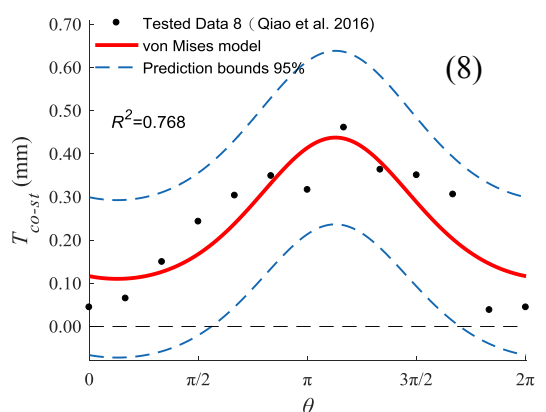
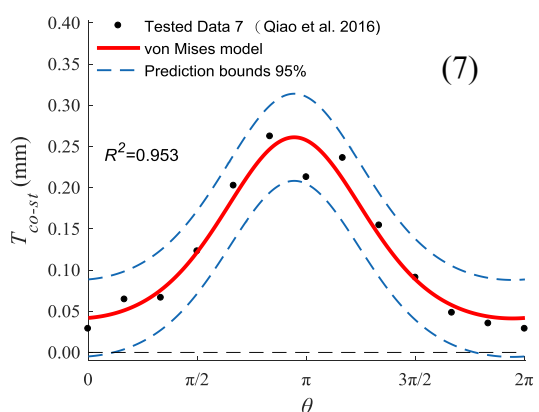
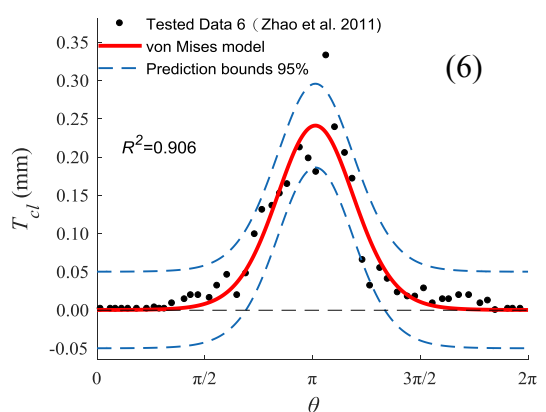
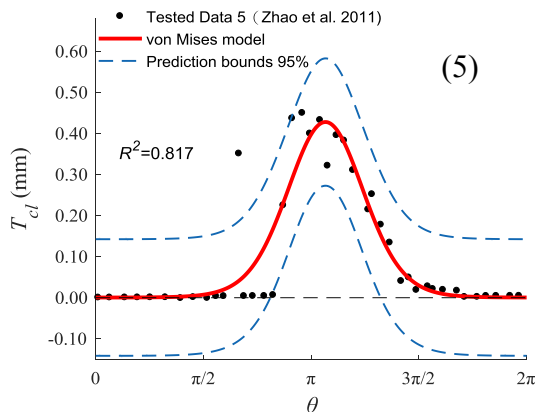
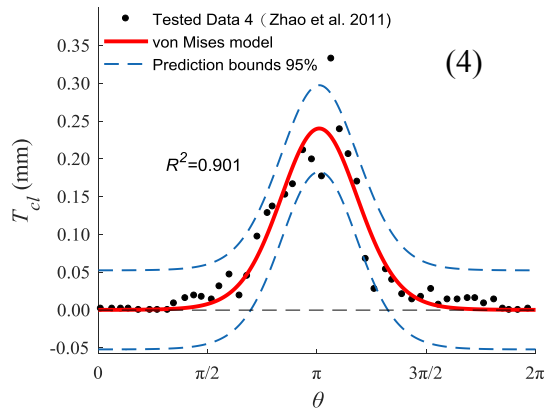
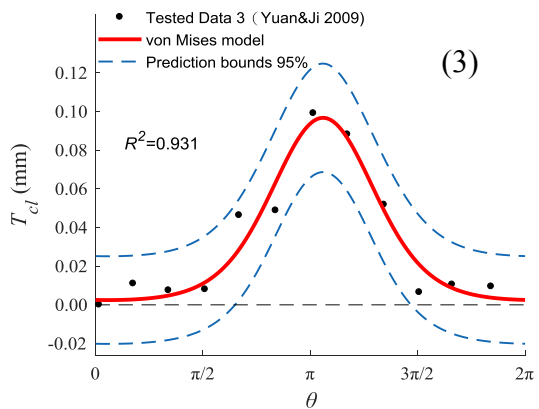
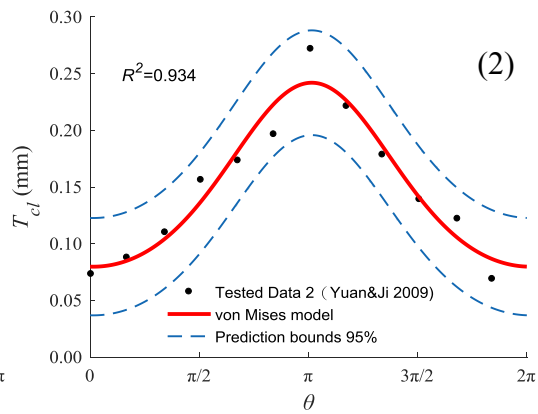
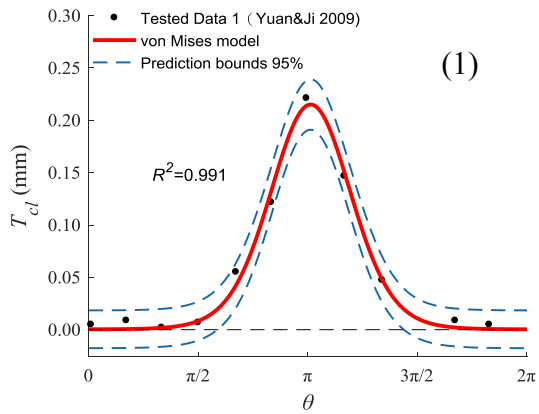
Table 4 Number of elements in the computational models

Model	Solid elements for mortar	Solid elements for aggregate	Cohesive elements for mortar	Cohesive elements for aggregate	Interfacial cohesive elements	Total
Middle rebar	12198	8174	15808	9996	4530	50706
Corner rebar	12422	8272	10058	16089	4700	51541

Table 5 Values for geometric and mechanical parameters for different phases

Description	Symbol	Values
Cover thickness	C	40 mm
Diameter of steel bars	D	16 mm
Young's modulus of aggregate	E_{Agg}	70 GPa [25]
Young's modulus of mortar	E_{Mor}	25 GPa [25]
Poisson's ratio of aggregate	ν_{Agg}	0.2 [25]
Poisson's ratio of mortar	ν_{Mor}	0.2 [25]
Tensile strength of mortar	$f'_{t,Mor}$	6 MPa [25]
Tensile strength of ITZ	$f'_{t,Int}$	3 MPa [25, 39, 40]
Fracture energy of mortar	$G_{f,Mor}$	60 N/m [25]
Fracture energy of ITZ	$G_{f,Int}$	15 N/m [25, 39, 40]

- 678 1. Various models on corrosion rust progression around the reinforcement in concrete
- 679 2. Regression analysis of the developed von Mises model with test data
- 680 3. Regression analysis of the existing models with test data
- 681 4. Comparison of average value of R^2 for various corrosion models
- 682 5. Polar coordinate system defined in experiments [15, 19, 23] and the developed model
- 683 6. Corrosion rust distributions based on the von Mises model under different values of k and
684 corrosion degree
- 685 7. Corrosion rust distributions based on the von Mises model under varying k and corrosion
686 degree
- 687 8. Expansion displacement T_d distributions under five different non-uniform coefficients
- 688 9. Meshes for concrete cover structures with middle rebar and corner rebar respectively
- 689 10. Inserted cohesive elements in the FE mesh
- 690 11. Constitutive relationship of concrete in tension
- 691 12. Crack propagation induced by corrosion of middle rebar for non-uniform coefficient $k=2$
- 692 13. Crack patterns under different corrosion non-uniform coefficient k
- 693 14. Surface crack width induced by corrosion of middle rebar as a function of corrosion
694 degree under different non-uniform corrosion coefficient k
- 695 15. Crack propagation induced by corrosion of corner rebar for non-uniform coefficient $k=2$
- 696 16. Crack patterns under different non-uniform corrosion coefficient k
- 697 17. Surface crack width induced by corrosion of corner rebar as a function of corrosion
698 degree η under different non-uniform coefficient k
- 699 18. Effect of the thickness of “porous zone” on crack pattern for non-uniform corrosion
700 coefficient $k=2$
- 701 19. Effect of the thickness of “porous zone” on the evolution of surface crack width



710

711

712

713

714

Figure 2 Regression analysis of the developed von Mises model with test data

715

(Note: the test data 4 and 6 were obtained from corrosion of corner rebar and the others were

716

from corrosion of middle rebar [15, 19, 23])

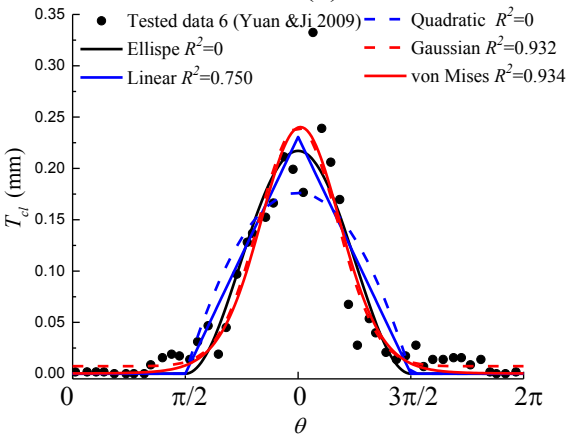
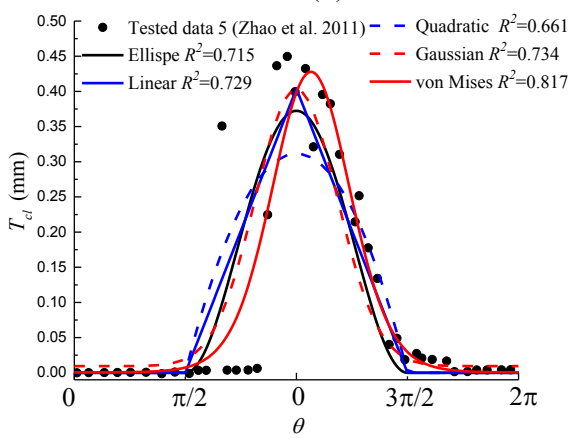
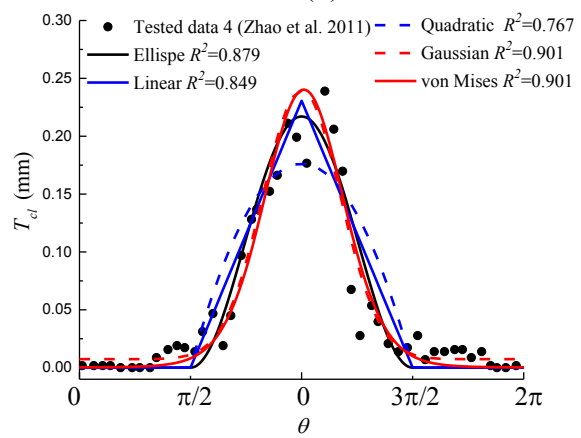
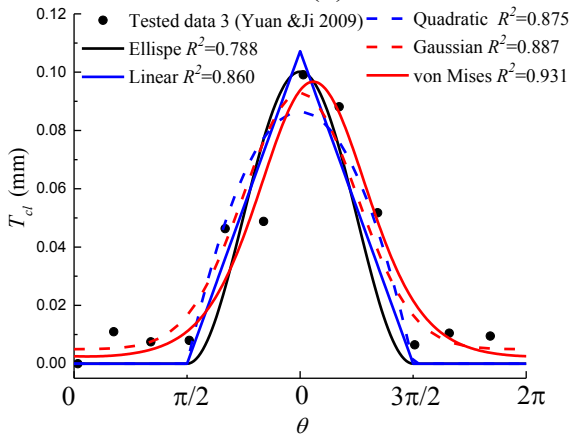
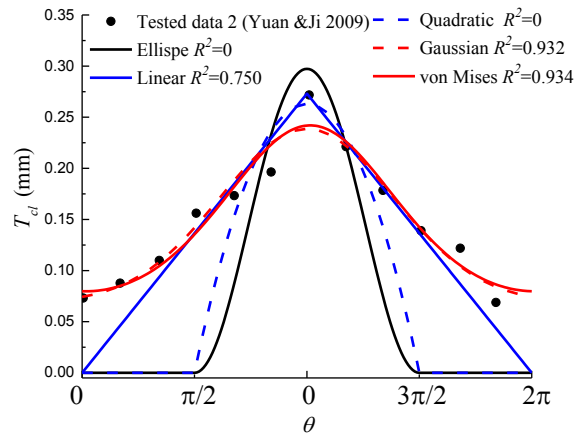
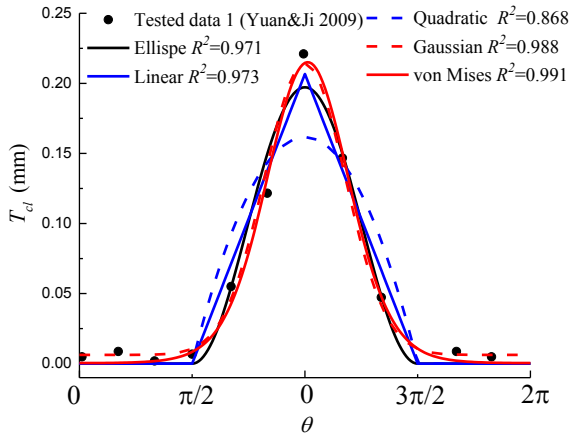
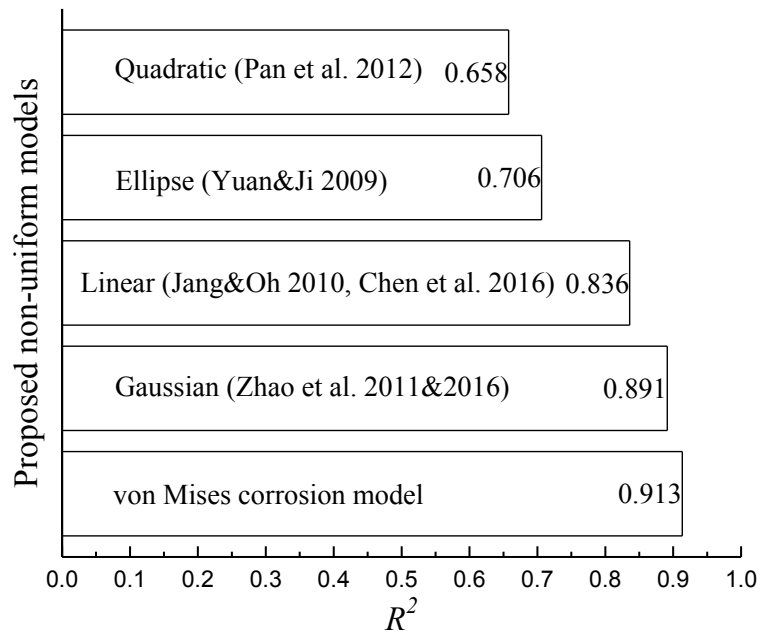


Figure 3 Regression analysis of the existing models with test data

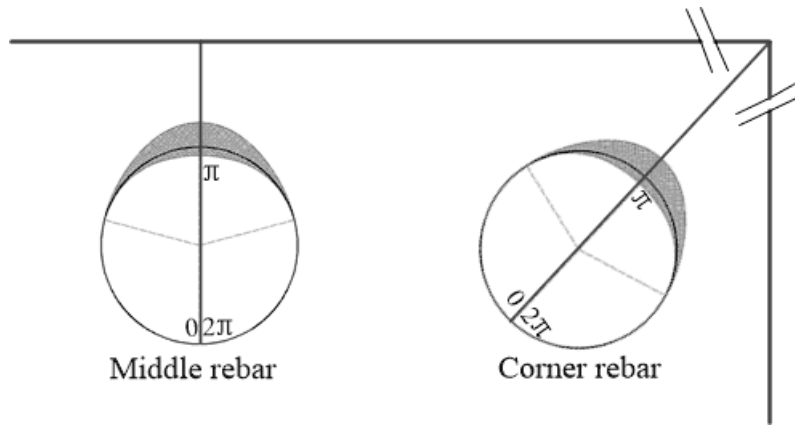


725

726

Figure 4 Comparison of average value of R^2 for various corrosion models

727



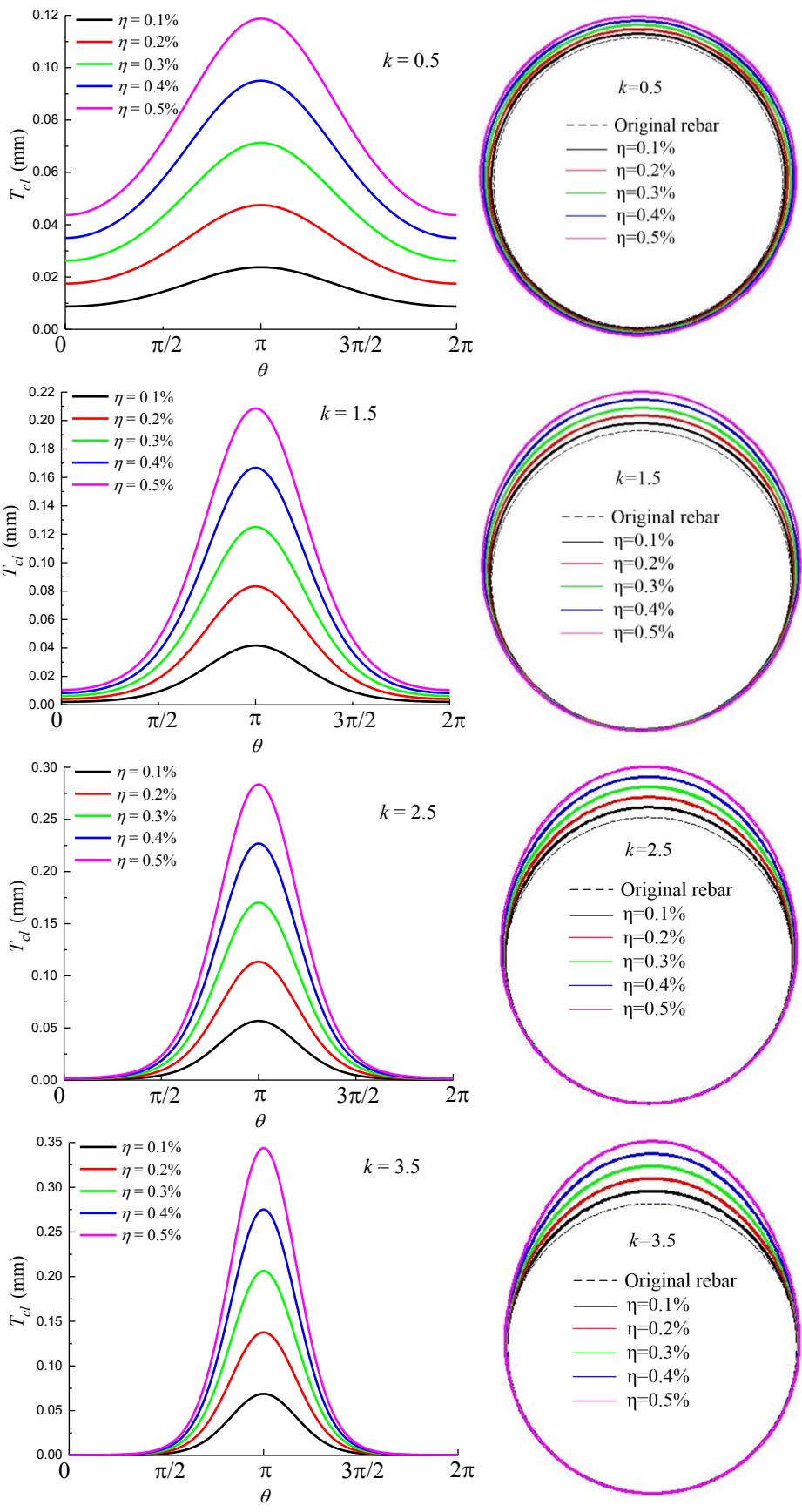
728

729 Figure 5 Polar coordinate system defined in experiments [15, 19, 23] and the developed

730 model

731

732



733

734

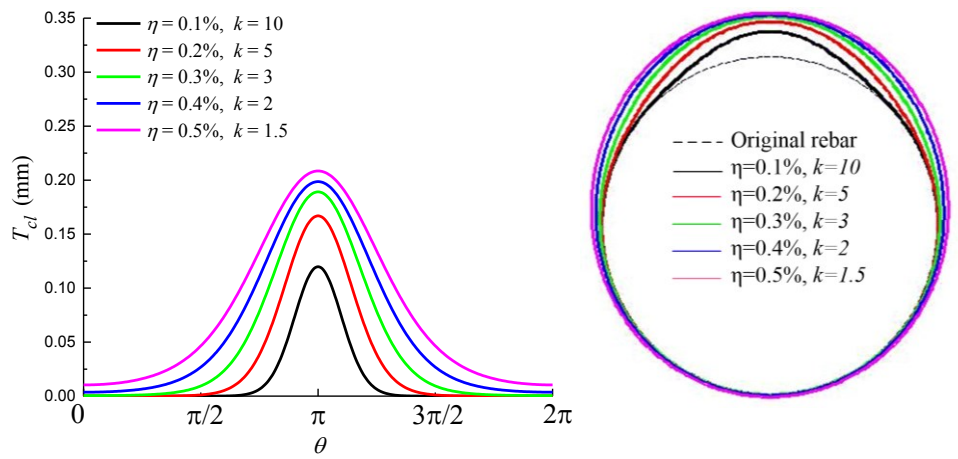
735

736

737

738

Figure 6 Corrosion rust distributions based on the von Mises model under different values of k and corrosion degree (Note: the deformation scale for the right pictures is 10)

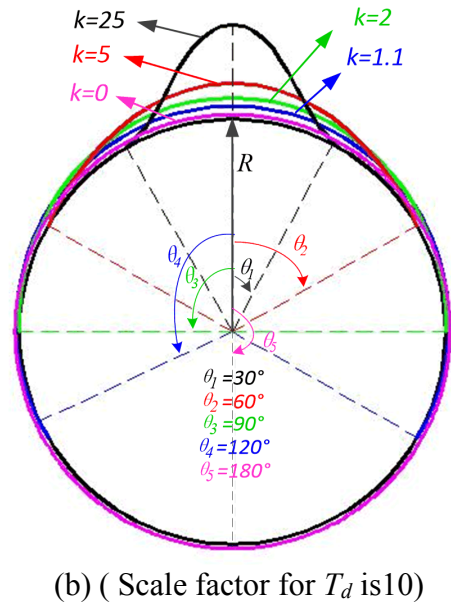
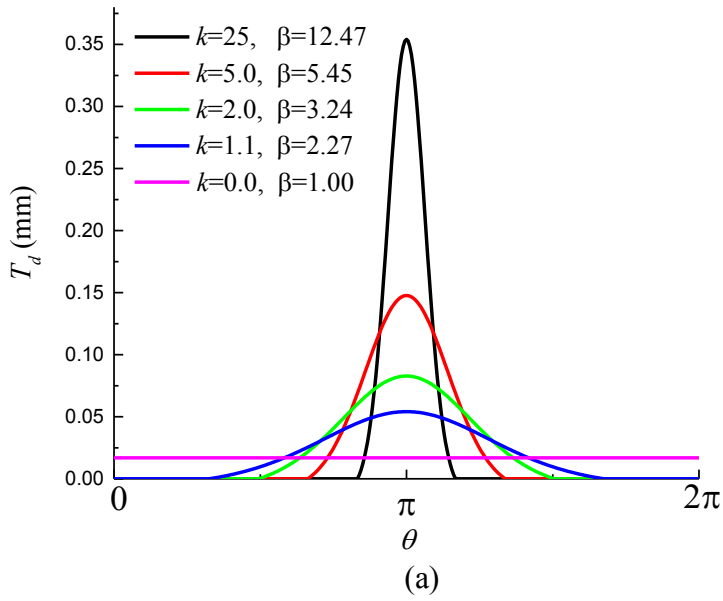


739

740 Figure 7 Corrosion rust distributions based on the von Mises model under varying k and

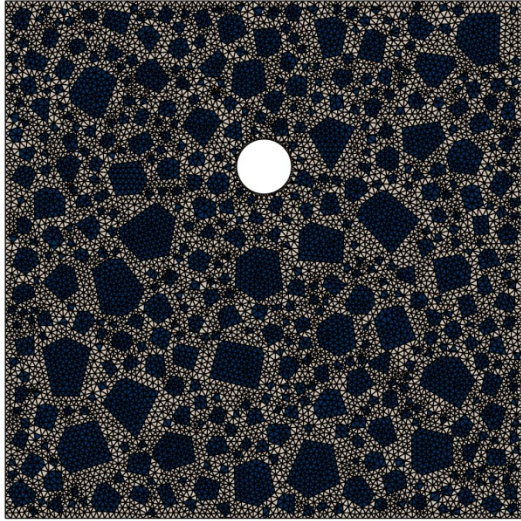
741 corrosion degree (Note: the deformation scale for the right picture is 10)

742

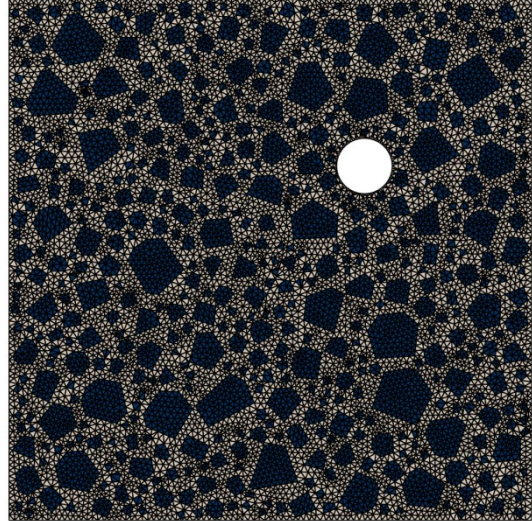


743
744
745
746
747

Figure 8 Expansion displacement T_d distributions under five different non-uniform coefficients



(a) Middle rebar



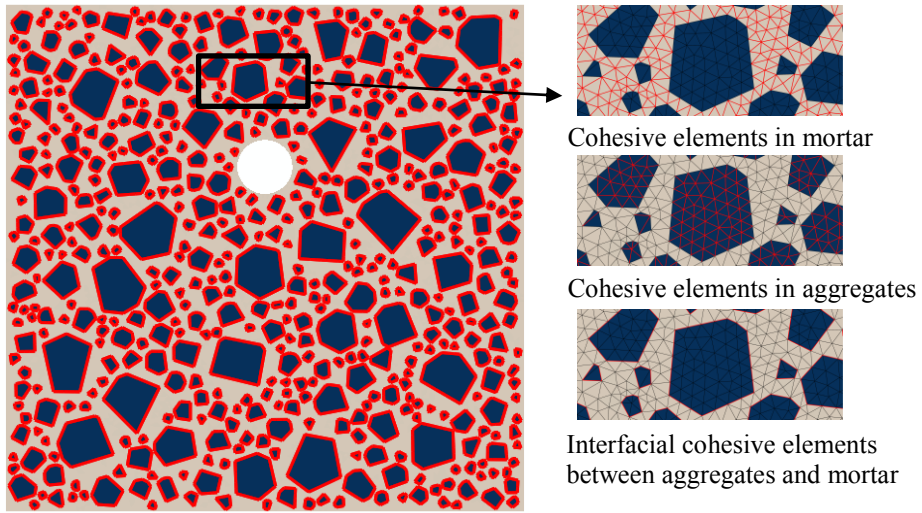
(b) Corner rebar

748
749

750
751
752

Figure 9 Meshes for concrete cover structures with middle rebar and corner rebar respectively

753

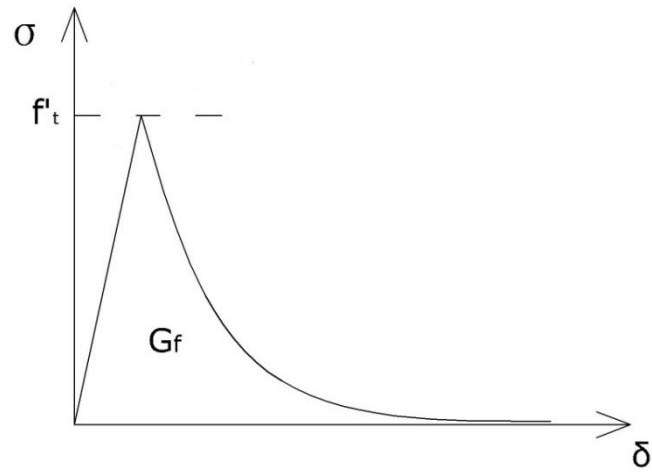


754

755

756

Figure 10 Inset cohesive elements in the FE mesh



757

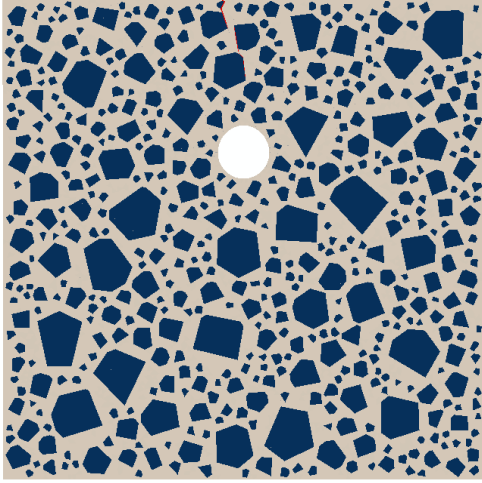
758

Figure 11 Constitutive relationship of concrete in tension

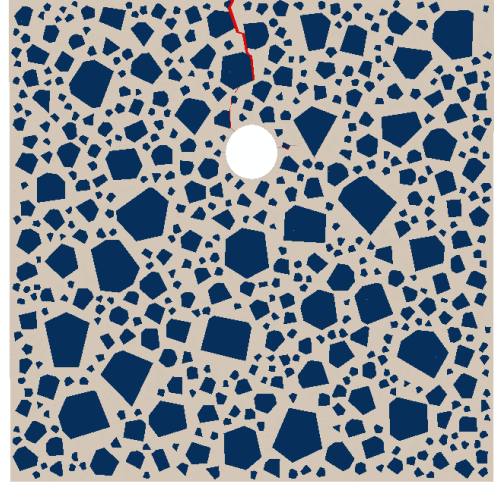
759

760

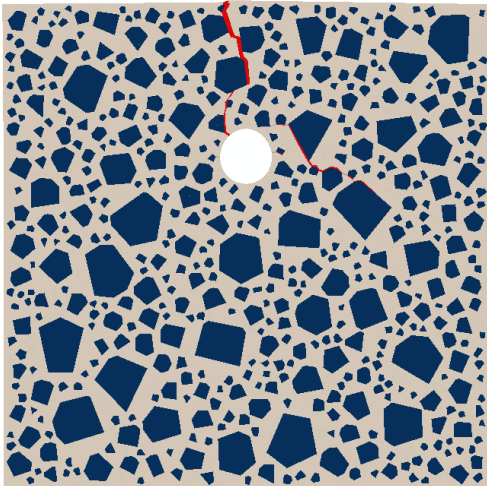
761
762



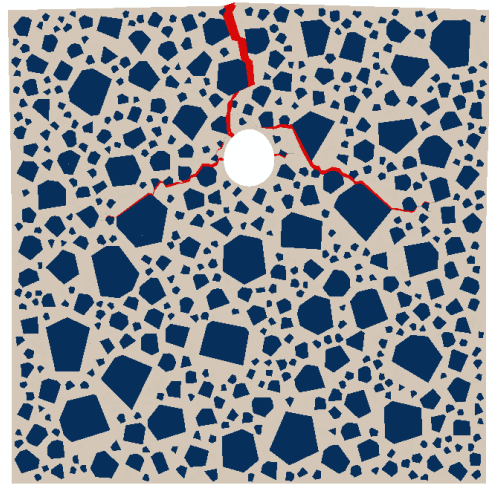
(a) corrosion degree $\eta = 0.11\%$



(b) corrosion degree $\eta = 0.12\%$



(c) corrosion degree $\eta = 0.15\%$

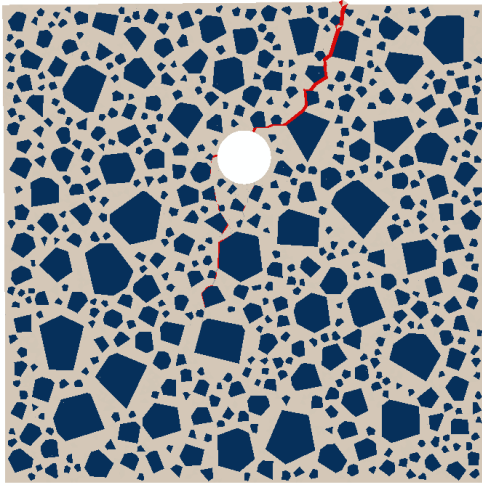


(d) corrosion degree $\eta = 0.26\%$

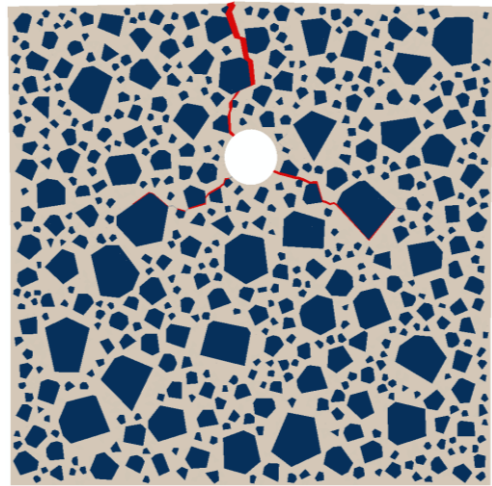
763
764
765
766
767
768

Figure 12 Crack propagation induced by corrosion of middle rebar for non-uniform coefficient $k=2$ (Note: the red regions represent completely cracked cohesive elements, i.e., $D = 1.0$; Deformation scale: 25)

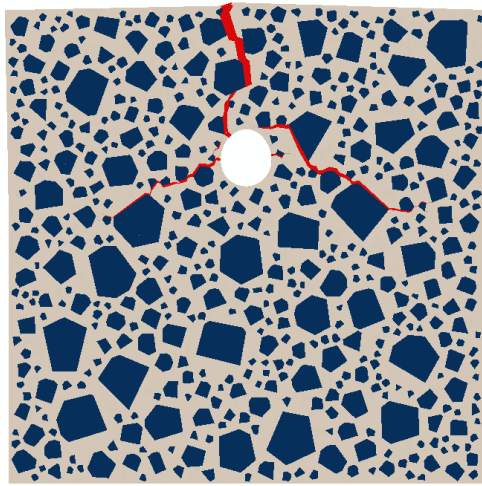
769
770



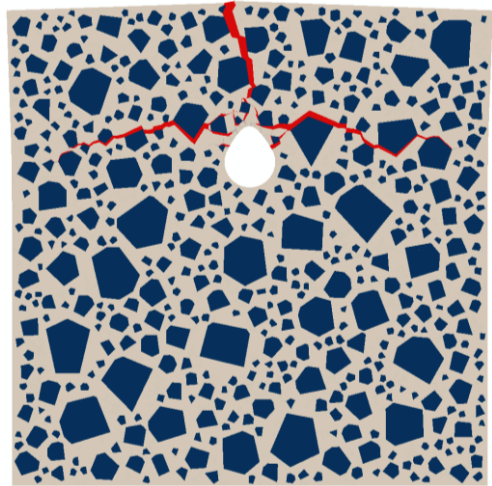
(a) $k = 0, \eta = 0.26\%$



(b) $k = 1.1, \eta = 0.26\%$

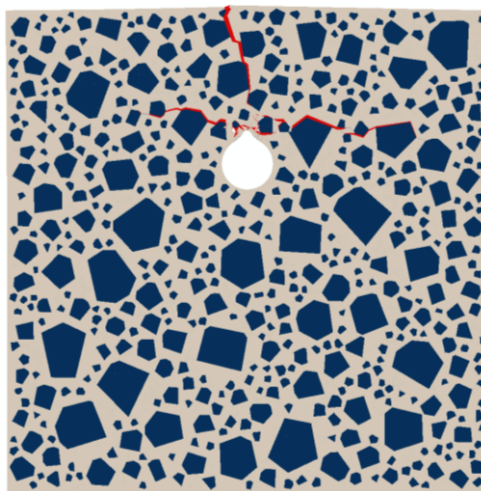


(c) $k = 2, \eta = 0.26\%$



(d) $k = 5, \eta = 0.23\%$

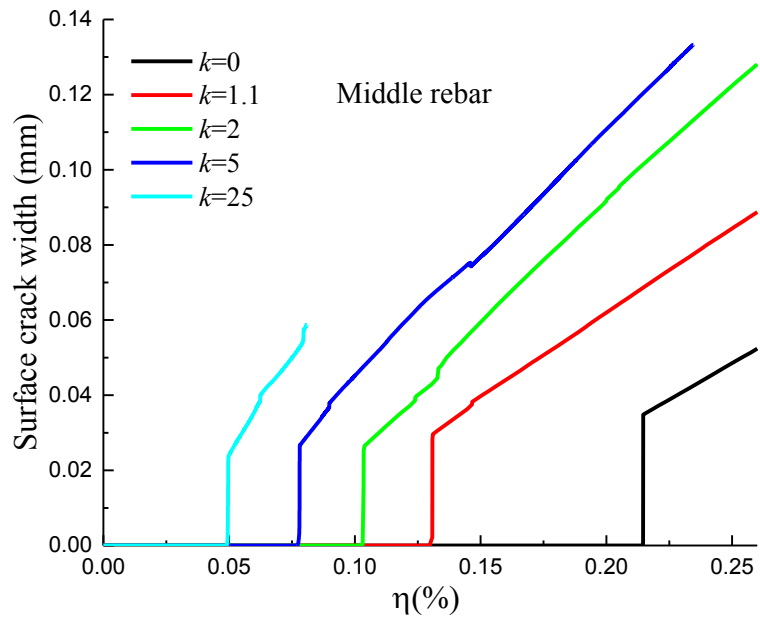
771
772



(e) $k = 25, \eta = 0.08\%$

773
774
775
776
777

Figure 13 Crack patterns under different corrosion non-uniform coefficient k
(Note: the red regions represent completely cracked cohesive elements, i.e., $D = 1.0$;
Deformation scale: 25)



778

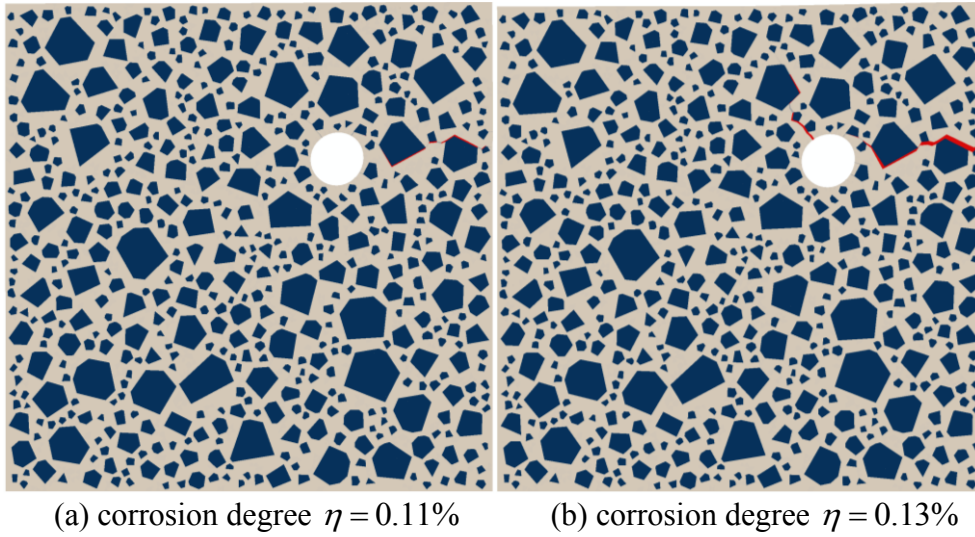
779

780

781

Figure 14 Surface crack width induced by corrosion of middle rebar as a function of corrosion degree η under different non-uniform corrosion coefficient k

782
783



784
785
786
787
788
789

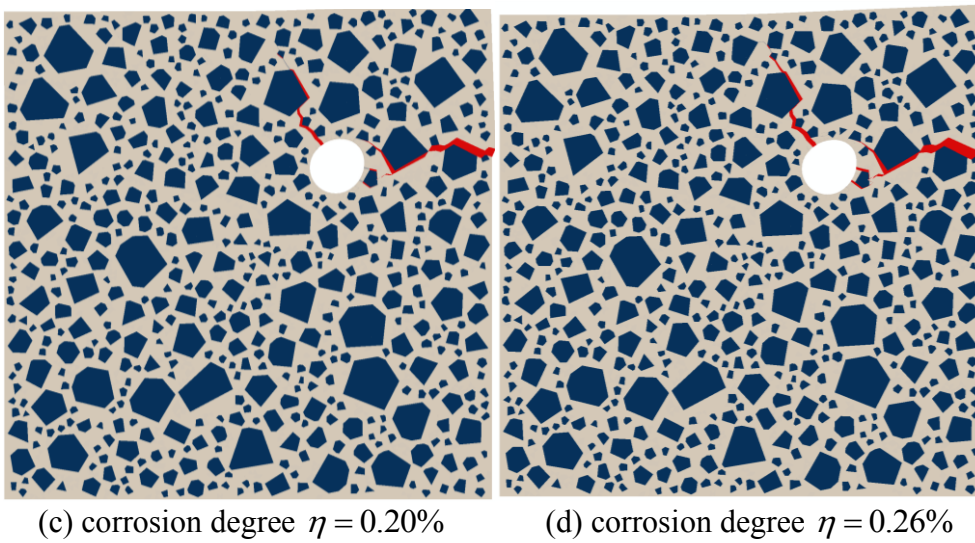
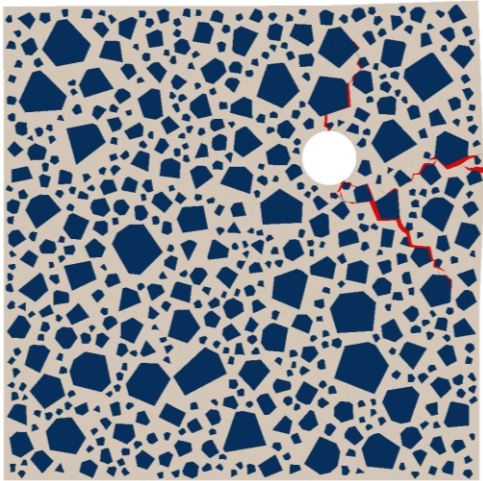
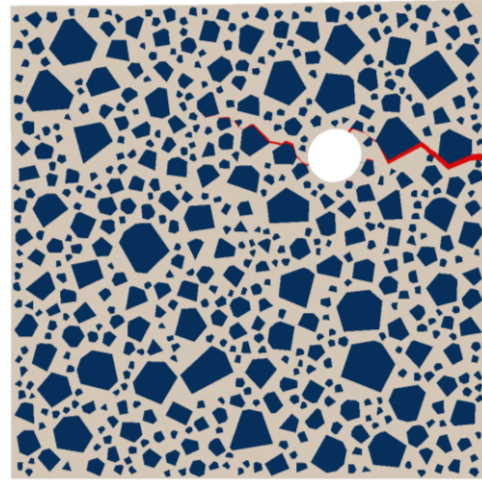


Figure 15 Crack propagation induced by corrosion of corner rebar for non-uniform coefficient $k=2$ (Note: the red regions represent completely cracked cohesive elements, i.e., $D = 1.0$; Deformation scale: 25)

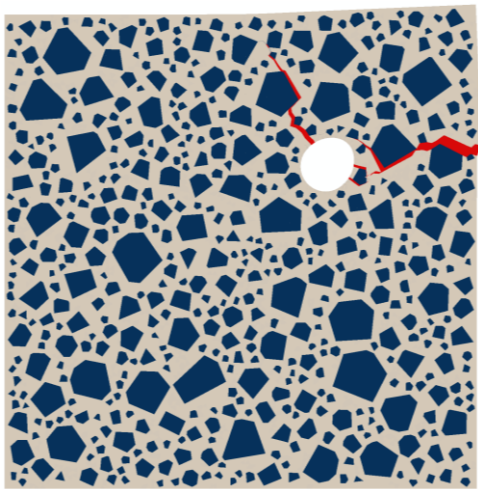
790
791



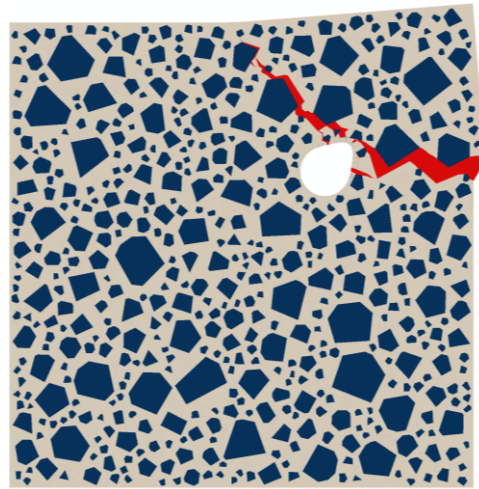
(a) $k = 0, \eta = 0.26\%$



(b) $k = 1.1, \eta = 0.26\%$

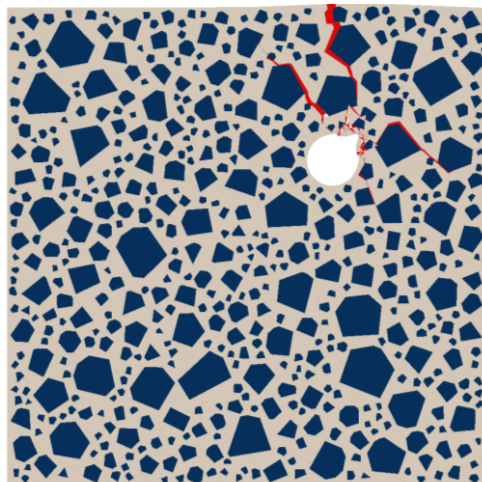


(c) $k = 2, \eta = 0.26\%$



(d) $k = 5, \eta = 0.26\%$

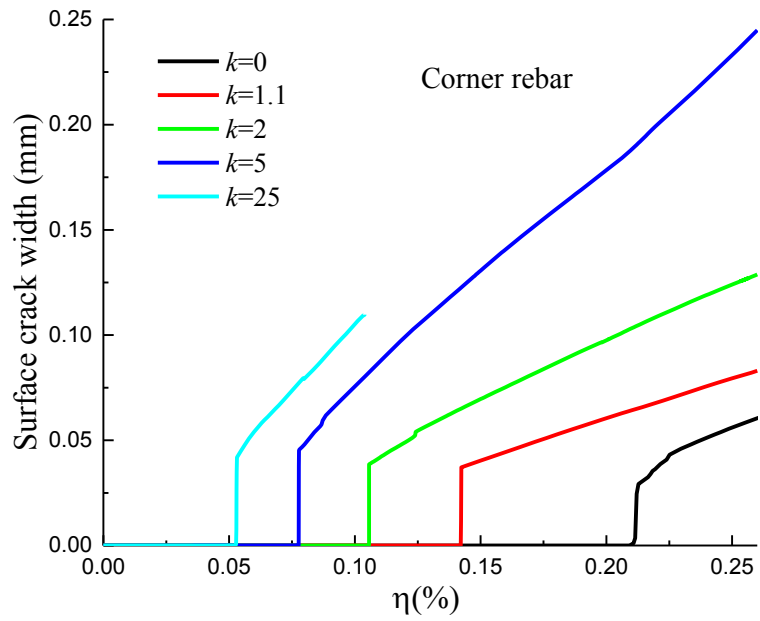
792
793



(e) $k = 25, \eta = 0.10\%$

794
795
796
797
798
799

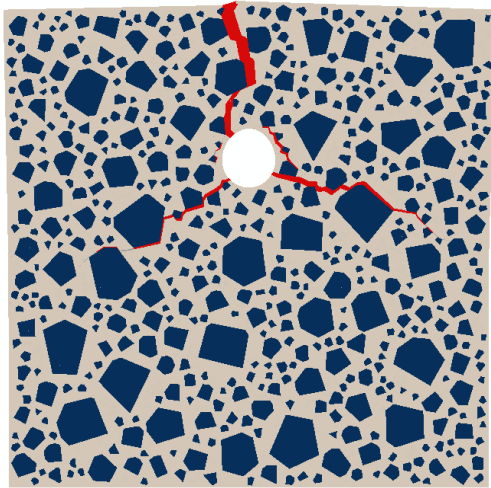
Figure 16 Crack patterns under different non-uniform corrosion coefficient k
(Note: the red regions represent completely cracked cohesive elements, i.e., $D = 1.0$;
Deformation scale: 25)



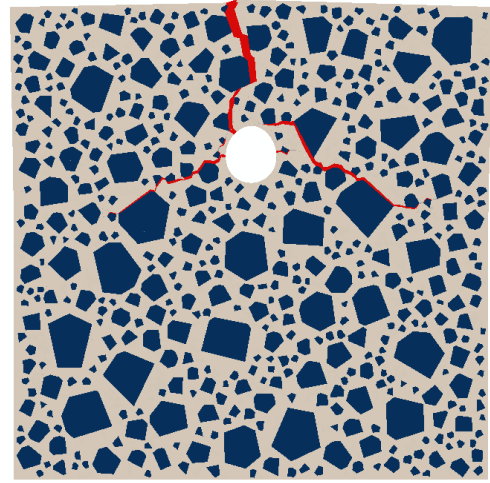
800
801
802

Figure 17 Surface crack width induced by corrosion of corner rebar as a function of corrosion degree η under different non-uniform coefficient k

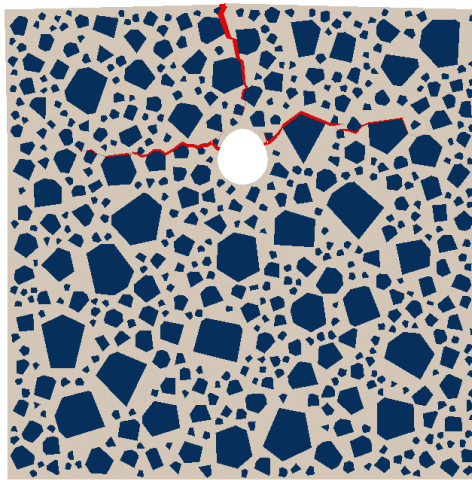
803
804



(a) $T_0=0$, $\eta = 0.26\%$



(b) $T_0=12.5 \mu\text{m}$, $\eta = 0.26\%$



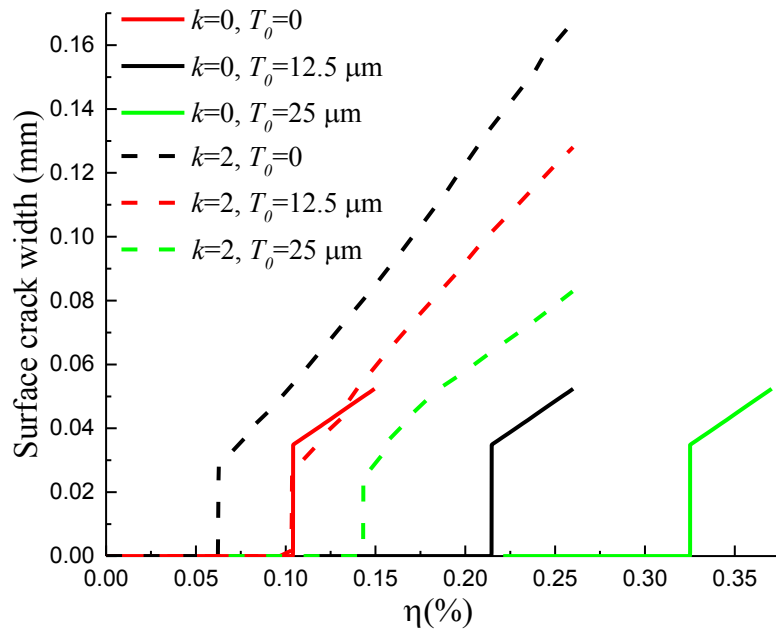
(c) $T_0=25 \mu\text{m}$, $\eta = 0.26\%$

805
806

807 Figure 18 Effect of the thickness of “porous zone” on crack pattern for non-uniform corrosion
808 coefficient $k=2$

809
810

811



812
813
814

Figure 19 Effect of the thickness of “porous zone” on the evolution of surface crack width